

# **EEG-Based Classification of Motor Imagery and Movement Across Brain Regions**

Sara Banimahdi Dehkordi<sup>1</sup>, <sup>2</sup>Abdul Rauf Anwar

<sup>1</sup>Department of Orthotics and Prosthetics, School of Rehabilitation, Medical School, Isfahan University of Medical Science, Iran.

<sup>2</sup>Uniklinikum RWTH Aachen, Aachen, Germany.

**Keywords:** Brain-Computer Interfaces (BCI), Machine Learning, Support Vector Machines, Brodmann areas

## **Abstract:**

The brain plays a crucial role in all actions, including motor imagery and movement. To better understand its function in these contexts, we utilize brain-computer interfaces. This study aims to enhance comprehension of brain activity during both imagined and actual motions, using this knowledge to inform neurorehabilitation strategies for individuals with movement impairments. An EEG dataset from 52 healthy participants performing motor imagery and hand movement tasks was analyzed. EEG signals were recorded using a 64-channel setup, with preprocessing involving noise filtering, artifact removal, and Principal Component Analysis (PCA) for dimensionality reduction. Features were extracted from temporal and spectral domains, and machine learning models, including Support Vector Machines (SVM), K-Nearest Neighbors (KNN), and Random Forest, were evaluated. The polynomial SVM yielded the highest accuracy (58.06%) and was used for further cortical region analysis. The parietal cortex demonstrated the best performance (58%), highlighting its role in sensorimotor integration. Although promising, further optimization of feature selection and model refinement is necessary. Future work should investigate region-specific improvements and applications in motor rehabilitation.

## **Description**

Motor imagery (MI)-based brain-computer interfaces (BCIs) have gained significant attention in recent years. Compared to other BCI paradigms, MI-based BCI enables communication without requiring limb movement or external stimuli. It utilizes “induced” rather than “evoked” brain activity (Pfurtscheller & Lopes da Silva, 1999). Imagined motor movement is crucial in learning and coordinating complex motor skills. Literature has shown its benefits in neurorehabilitation,

particularly for stroke patients and prosthesis users, enhancing their ability to control movements more effectively (Miller et al., 2010).

While many prior studies on MI-based BCI have focused on specific motor regions such as the primary motor cortex, there remains a gap in understanding the involvement of other cortical areas during imagined and actual movements. Exploring broader cortical engagement can offer insights into how the brain processes movement, whether through thought or action. This study investigates multiple brain areas in a single dataset to better understand the distribution of motor-related brain activity, aiming to inform improved neurorehabilitation strategies. For this, we utilized an EEG dataset from 52 healthy individuals collected by Cho et al., available in the GigaScience database (Cho et al., 2017).

Each participant completed at least 100 trials involving both motor imagery and actual hand movements. EEG data were recorded using 64 Ag/AgCl active electrodes in a 64-channel montage adhering to the international 10-10 system, with a sampling rate of 512 Hz. We focused on electrodes over four cortical regions: Primary Motor Cortex (Brodmann Area 4): C3, C4, CZ; Premotor Cortex (Brodmann Area 6): FC3, FC4, FCZ; Posterior Parietal Cortex (Brodmann Areas 5 and 7): CP3, CP4, CPZ, PZ, P3, P4; and Temporal Cortex (Brodmann Areas 20, 21, and 22): T7, T8. To ensure data quality and reduce noise, we applied a 60 Hz notch filter using an infinite impulse response (IIR) filter with a quality factor of 30. The normalized frequency was based on the EEG sampling rate, and zero-phase filtering was applied using the `filtfilt` function to avoid phase distortions. The notch filter was applied independently to each EEG channel to maintain signal integrity.

Following artifact removal and filtering, we performed PCA to reduce dimensionality. The principal components were calculated, and cumulative variance was analyzed to retain 95% of the total variance while reducing the feature space. The optimal number of components was chosen where the cumulative variance exceeded the 95% threshold. To standardize the feature space and aid model convergence, we applied Min-Max Normalization, rescaling feature values to the [0,1] range to ensure equal contribution from each feature.

To support robust preprocessing and analysis, we employed EEGLAB in MATLAB, which enabled efficient management of large datasets and extraction of meaningful patterns. Averaged

Power Spectral Density (PSD) across selected electrodes was used to evaluate power fluctuations across frequency bands. We applied machine learning algorithms, including Support Vector Machine (SVM), K-Nearest Neighbor (KNN), and Random Forest, to determine the most effective classification approach.

Feature extraction involved frequency-domain features from alpha, beta, theta, and gamma bands and time-domain features such as mean, variance, skewness, and entropy. Hjorth parameters were also used to evaluate EEG signal complexity and mobility. The dataset was divided into training and testing subsets using a 70-30 split to ensure balanced evaluation. Although the original EEG dataset included four distinct conditions (right and left imagery, right and left actual movement), we grouped them into two categories: motor imagery and actual movement. This allowed us to focus on the key differences between these conditions relevant to our study.

To compute overall classification accuracy, we tested various electrode combinations from the four cortical areas and identified the most reliable electrodes: C3, CZ, FC3, FCZ, CP3, CPZ, P3, PZ, T7, and T8. We also conducted region-specific analyses by examining accuracy within each cortical region based on Brodmann areas. Both overall and regional accuracy provided information about brain activity patterns relevant to our objectives.

To identify the most effective machine learning model, we evaluated several algorithms, focusing on optimizing SVM kernels. We tested three SVM kernels: linear, polynomial, and Radial Basis Function (RBF), and compared them with Random Forest. Model performance was assessed using confusion matrices. In Figure 1.A, the confusion matrix displays results for the polynomial kernel SVM. The diagonal values (4 and 14) represent correct classifications, while off-diagonal values (11 and 2) indicate errors. The model correctly classified 87.5% of imagery movement instances (Class 2) but misclassified 73.3% of actual movement instances (Class 1). Accuracy results were as follows: Linear SVM: 38.71%, Polynomial SVM: 58.06%, RBF SVM: 51.61%, and Random Forest: 48.3%. The polynomial SVM, with the highest accuracy, was selected for further analysis.

These findings suggest that EEG data likely possess a non-linear structure that the polynomial kernel effectively models. Polynomial transformations enable the model to learn complex decision boundaries influenced by neural dynamics and sensor noise. Although Random Forest

can model non-linear relationships through ensembles of decision trees (Breiman, 2001), its lower performance in this study may be due to the EEG data's noisiness and the dataset's limited size (52 participants with around 100–120 trials each). These limitations can cause Random Forest to overfit to individual-specific noise or patterns that do not generalize well. In contrast, kernel-based methods like polynomial SVM can better capture subtle, high-dimensional decision boundaries.

We evaluated SVM classification performance in specific cortical areas. Accuracy rates were 55% for the primary motor cortex (BA 4), 48% for the premotor cortex (BA 6), 58% for the parietal cortex (BA 5 and 7), and 48% for the temporal cortex (BA 20–22). These sub-60% accuracy levels may be due to remaining noise, artifacts, or characteristics of feature selection. Despite preprocessing, EEG signals are susceptible to contamination, and alternative feature selection strategies might yield improved outcomes.

A key finding was the relatively high classification accuracy in the parietal cortex (58%), supporting its crucial role in somatosensory integration and spatial representation during both imagined and executed movements. The temporal cortex also contributed (48%), consistent with its involvement in visualizing and imagining body movements. The roles of the temporal cortex and BA 4 suggest complementary contributions to imagined and actual movements.

To better interpret regional classification performance, we used a 3D surface plot to visualize accuracy across Brodmann areas. In this plot, areas like BA 4 and BA 7 appear in red, indicating higher classification accuracy, while areas such as BA 5 and BA 20–22 are shown in blue, reflecting lower performance. This visualization reinforces the idea that certain cortical regions are more influential in distinguishing motor-related brain states (Figure 1.B).

We extended our analysis by calculating per-class accuracy, which offered further insight into model performance across the two movement types. Motor imagery (Class 2) achieved higher accuracy than actual movement (Class 1), a pattern also reflected in the polynomial SVM confusion matrix (Figure 1.A), confirming it as the best-performing model (Figure 1.C).

To refine our classification analysis, we explored feature ranking to identify the most informative input variables. While the Random Forest model offered clarity in ranking frequency-domain

features, interpreting importance within the non-linear polynomial SVM model was more challenging. Therefore, we preserved all selected features to maintain a comprehensive analysis framework.

In summary, while SVM models provided acceptable performance, improvements in signal processing and feature selection could further enhance classification accuracy. Future research should focus on refining classification within targeted cortical regions and optimizing electrode configurations. Additionally, distinguishing between left and right hand imagery and movement remains a valuable direction, particularly for unilateral motor rehabilitation. Expanding the dataset to include a more diverse population or increasing trial counts may also improve model generalizability. Finally, the application of deep learning or hybrid models could better capture the spatial-temporal dynamics of EEG signals.

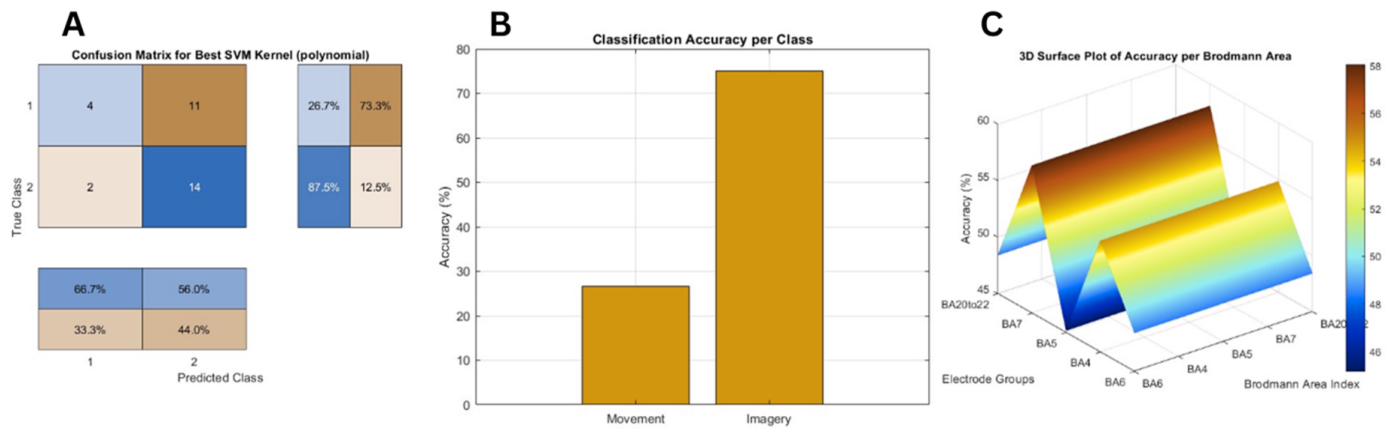


**Figure 1**

**(A) Confusion matrix for the best-performing SVM with a polynomial kernel, showing absolute values, row-wise normalization (right), and column-wise normalization (bottom).**

**(B) Classification Accuracy per Class.**

**(C) 3D Surface Plot of Accuracy per Brodmann Area.**

## Acknowledgements

I sincerely thank my mentor, Dr. Rauf Anwar, for their invaluable guidance, encouragement, and insightful feedback throughout this research. Their support has been instrumental in shaping this study. I would also like to acknowledge my group members, Daksh Mehta, Navid Noroozi, and Suvadeep Maiti, for their collaboration and contributions to this project.

## References

- Breiman, L. (2001). Random Forests. *Machine Learning*, 45, 5–32.  
<https://doi.org/10.1023/A:1010933404324>
- Cho H, Ahn M, Ahn S, & Kwon M. (2017). Supporting data for “EEG datasets for motor imagery brain computer interface” *GigaScience Database* [Dataset].  
<https://doi.org/10.5524/100295>
- Cho, H, H., Ahn, M, Ahn, S, & Moonyoung Kwon. (2017). EEG datasets for motor imagery brain-computer interface. *Gigascience*, 6(7). <https://doi.org/10.1093/gigascience/gix034>
- G. Pfurtscheller, & F.H. Lopes da Silva. (1999). Event-related EEG/MEG synchronization and desynchronization: Basic principles. *Clinical Neurophysiology*, 110(11), 1842–1857.  
[https://doi.org/10.1016/s1388-2457\(99\)00141-8](https://doi.org/10.1016/s1388-2457(99)00141-8)
- K.J. Miller, G. Schalk, E.E. Fetz, M. den Nijs, & J.G. Ojemann. (2010). Cortical activity during motor execution, motor imagery, and imagery-based online feedback. *Proc Natl Acad Sci USA*. <https://doi.org/10.1073/pnas.0913697107>